NANO LETTERS

pubs.acs.org/NanoLett

On the Correlation between Nanoscale Structure and Magnetic Properties in Ordered Mesoporous Cobalt Ferrite ($CoFe_2O_4$) Thin Films

Thomas E. Quickel,[†] Van H. Le,[†] Torsten Brezesinski,[†,‡] and Sarah H. Tolbert*[,†]

[†]Department of Chemistry and Biochemistry, University of California at Los Angeles, Los Angeles, California 90095-1569 and [‡]Institute of Physical Chemistry, Justus-Liebig-University Giessen, Heinrich-Buff-Ring 58, 35392 Giessen, Germany

ABSTRACT In this work, we report the synthesis of periodic nanoporous cobalt ferrite (CFO) that exhibits tunable room temperature ferrimagnetism. The porous cubic CFO frameworks are fabricated by coassembly of inorganic precursors with a large amphiphilic diblock copolymer, referred to as KLE. The inverse spinel framework boasts an ordered open network of pores averaging 14 nm in diameter. The domain sizes of the crystallites are tunable from 6 to 15 nm, a control which comes at little cost to the ordering of the mesostructure. Increases in crystalline domain size directly correlate with increases in room temperature coercivity. In addition, these materials show a strong preference for out-of-plane oriented magnetization, which is unique in a thin film system. The preference is explained by in-plane tensile strain, combined with relaxation of the out-of-plane strain through flexing of the mesopores. It is envisioned that the pores of this ferrimagnet could facilitate the formation of a diverse range of exchange coupled composite materials.

KEYWORDS Cobalt ferrite, mesoporous, polymer templating, nanomagnetics, EISA

Magnetic materials are the focus of much research and development due to the integral role they play in high-density data storage. In particular, advances that receive widespread attention are those that broaden the scope of magnetic materials in the technology arena. Examples of these types of materials include nanosized room temperature ferromagnets for memory applications or materials with high magnetization and switchability that lend themselves to thin film architectures for device development.

It is well documented that as magnetic materials approach the nanoscale regime, their properties begin to differ from their bulk counterparts. For example, as the sizes are reduced, magnetic nanoparticles approach the superparamagnetic limit where ambient thermal energy can randomize the magnetization. This phenomenon leads to nanomaterials with zero coercivity and zero remanent magnetization.[1] For many applications where weak ferromagnetism is required, it is desirable to design nanomagnets that retain high magnetization, nonzero coercivity, and remanence.

The ability to reduce a bulk magnetic material to the nanoscale size while preserving its innate ferromagnetic character is of great importance when developing magnetic data storage devices. Many methods have been utilized to produce films of magnetic material with nanoscale structures. For example, thin film nanoscale magnetic materials have been successfully produced via electrodeposition,[2] sol gel techniques,[3] and plasma laser deposition (PLD).[4] The range of nanoscale magnetic materials extends far beyond thin films as nanorods,[5,6] nanocrystals,[7−9] ordered nanocrystal arrays,[10,11] and nanocrystal superlatices[12] can also be readily formed. Even mesoporous monoliths have been generated from magnetic phases, such as MFe_2O_4 (M = Fe, Ni, Mn), through sol gel techniques.[13−15] Transition metal oxides such as the ferrites are particularly useful as they combine interesting magnetic and electrical properties with stability against oxidation. Thus, these ferrites constitute an important class of materials that are used extensively in the field of magnetic memory.[16] Cobalt ferrite, $CoFe_2O_4$ (CFO), a ferrimagnetic inverse spinel, is the most commercially significant member of the magnetic ferrites class. It is the common material of choice used in magnetic video and audio recording tapes and serves as a ferromagnetic component of read/write heads.[17]

CFO also has a rich presence in composite multiferroic materials. Such materials exhibit the magnetoelectric effect (ME) wherein electric polarizations are controllable through magnetic means or, alternatively, where electric fields are used to control magnetic polarizations. Much of the coupling between these two order parameters relies on strain effects that arise when piezoelectric materials are partnered with magnetostrictive ferromagnets.[18−20] In these multiferroic composites, the magnetic properties are altered through

* Corresponding author, tolbert@chem.ucla.edu.
Received for review: 04/22/2010
Published on Web: 00/00/0000

DOI: 10.1021/nl1014266 | *Nano Lett.* **XXXX,** *xxx,* 000–000

stress imparted by the electrically biased piezoelectric material.[21] Of the ferrites family, CFO expresses the highest degree of magnetostriction,[22] thus making it an attractive ferrimagnetic candidate for composite multiferroics. Due to the commercial importance of CFO, many groups have employed an assortment of methods to produce phase pure CFO particles,[23−25] rods,[26] and wires[27] on the nanoscale size.

Surfactant and polymer templating of inorganic materials is a facile route to produce porous materials with three-dimensional nanoscale architecture.[28−32] The fabrication of these mesoporous structures in thin film format using solution phase chemistry has become widespread since Ogawa, Brinker, and others published their seminal papers in the late 1990s, giving birth to the ever-growing field of evaporation-induced self-assembly (EISA).[33,34] To date, many important, metal oxides have been made through this method.[35−38] The use of EISA to produce magnetic phases in general and CFO with a three-dimensional interconnected nanoscale architecture in specific, however, has not been reported. The work presented here is thus the first step in uniting the versatile chemistry of polymer-templated porous materials with the technologically exciting field of magnetic materials.

The intricacies of the EISA techniques are well established and can be directly applied to the synthesis of CFO.[34,39] While various block copolymers can be used to create cubic, hexagonal, or lamellar architectures, the polymer employed here has a strong propensity to form a network with cubic pore symmetry.[41−43] There are many commercially available polymers that can be used to produce porous nanoscale frameworks with small and medium pore sizes. Because the wall thickness in these materials is small compared to the stable critical nucleation size, however, a loss of order in the framework is typically observed at the onset of crystallization. To circumvent this issue, a large diblock copolymer of the KLE family, poly(ethylene-*co*-butylene)-*b*-poly(ethylene oxide) was used as the template. KLE has a rich presence in the literature as it has been used to produce many highly crystalline metal oxides that possess well-defined nanoscale periodicity.[40−42] Part of the reason for this is the formation of inorganic−organic composites with sufficiently thick pore walls that they can be fully crystallized readily.

In the present work, we use EISA to produce a novel mesoporous ferrimagnet with ordered cubic network of pores. Unlike CFO nanoparticles with similar crystalline domain sizes which show superparamagnetic character,[23] these CFO porous frameworks are room temperature ferrimagnets. Furthermore, the mesoporous CFO films display a strong perpendicular magnetization which is uncommon in dense thin films. This observation suggests that the nanoscale architecture can be used to impart magnetic anisotropy in the mesoporous CFO material.

Experimental Section. ***Materials.*** $Fe(NO_3)_3 \cdot 9H_2O$ (99.9%) and $Co(NO_3)_2 \cdot 6H_2O$ (99.9%) were purchased from Sigma-Aldrich. $H[(CH_2CH_2)_{0.67}(CH_2(CH)CH_2CH_3)_{0.33}]_{89}$-$[OCH_2CH_2]_{79}OH$ (also referred to as KLE-22) was used as the organic template.

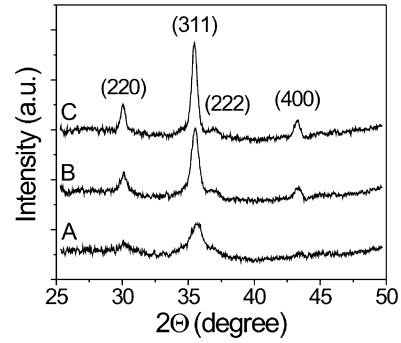

FIGURE 1. High-angle XRD patterns obtained on mesoporous $CoFe_2O_4$ samples heated to 500 (A), 600 (B), and 700 °C (C).

Synthesis. In a typical synthesis, both $Fe(NO_3)_3 \cdot 9H_2O$ (0.31 g) and $Co(NO_3)_2 \cdot 6H_2O$ (0.11 g) are dissolved in 1 mL of 2-methoxyethanol, 1 mL of EtOH, and 0.02 mL of glacial acetic acid. Once the solution is homogeneous, KLE polymer (0.04 g) dissolved in 1 mL of EtOH is added, for a total sol volume of roughly 3 mL. The solution was then allowed to clarify by magnetic stirring for 1 h. Films were dip-coated from the solution onto silicon wafers in a humidity-controlled chamber set to ∼17% relative humidity. The withdrawal rate varied between 1 and 2 cm/min depending on desired thickness. The films were calcined under air at 250 °C for 24 h to form rigid inorganic/organic composite structures. Crystallization and subsequent removal of the organic template were achieved by heating the films above 500 °C using a 10 °C/min ramp rate.

Methods. In- and out-of-plane high-angle X-ray diffraction (XRD), 2D small-angle X-ray scattering (2D-SAXS), field emission scanning electron microscopy (FESEM), and SQUID magnetometry were conducted to characterize the samples. Conventional high-angle XRD was measured using a D8-GADDS diffractometer from Bruker instruments (Cu Kα radiation). 2D-SAXS and angular-dependent high angle XRD data were collected at the Stanford Synchrotron Radiation Laboratory using beamlines 1-4 and 7-2, respectively. FE-SEM images were obtained using a JEOL 6700F instrument. Magnetic measurements were carried out on a Quantum Design MPMS 5T SQUID magnetometer with RSO detection.

Results and Discussion. To ensure that all magnetic characteristics of the film can be associated with the desired inverse spinel phase of ferrimagnetic CFO, we used high-angle X-ray diffraction to examine the crystallized films (Figure 1). It was observed that the samples formed the inverse spinel $CoFe_2O_4$ in phase pure form as corroborated with JCPDS reference card #22-1086. The films begin to crystallize at 500 °C as indicated by the emergence of the most intense (311) peak. Scherrer analysis of the crystallite grain size indicates that the grains grow as the temperature is increased. Crystalline domain size starts at 6 nm at 500 °C and reached 15−16 nm at 700 °C.

DOI: 10.1021/nl1014266 | *Nano Lett.* **XXXX,** *xxx,* 000−000

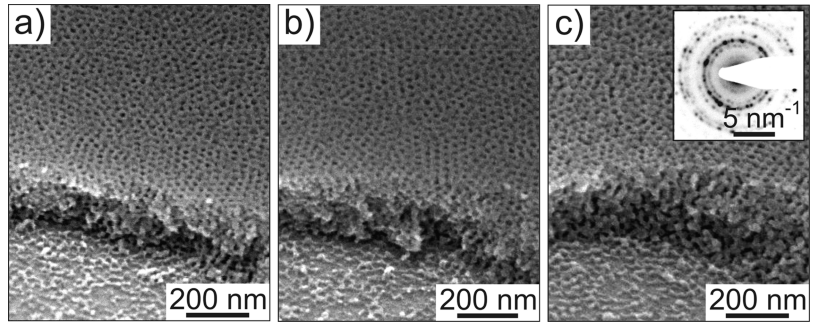

FIGURE 2. SEM images of a cut in a KLE-templated $CoFe_2O_4$ film heated to 250 (a), 500 (b), and 700 °C (c). An electron diffraction pattern of the sample shown in (c) is shown in the inset. The lattice spacings correspond well with inverse spinel CFO.

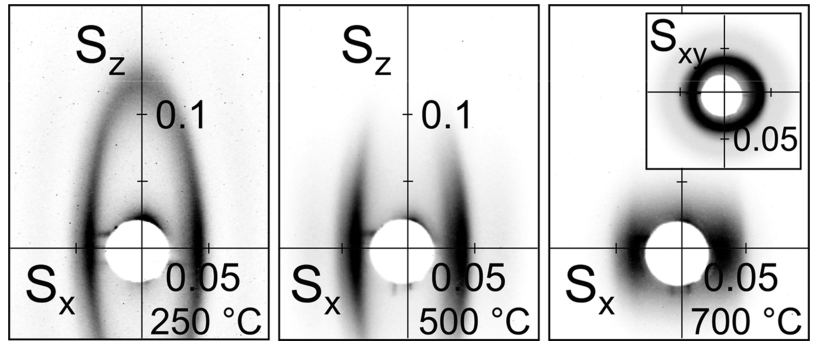

FIGURE 3. 2D-SAXS patterns obtained on a KLE-templated $CoFe_2O_4$ thin film heated to different annealing temperatures. Data were collected at an angel of incidence, β, of 10° and show the evolution of the distorted cubic network upon thermal treatment. A pattern taken in transmission mode, i.e., at $\beta = 90°$, is shown in the inset. Scattering vector s components are given in 1/nm.

To probe the mesoporous architecture, FESEM was used to image the films. The samples were oriented at 45° so that both the top surface of the film and the porous interior could be imaged simultaneously. Figure 2a shows the amorphous framework after calcination at 250 °C for 24 h. We note that at this point some KLE polymer is still present inside the pores. Upon heating to temperatures above 450 °C (not shown), the KLE polymer is combusted, leaving behind a fully cross-linked, amorphous metal oxide framework with an ordered cubic network of open pores.

As shown in Figure 1, the onset of CFO crystal growth occurs at 500 °C with the crystalline grain size increasing up to 700 °C. Thus, the nanoscale architecture must be able to survive such extreme heat treatments to preserve the mesoporous structure while enhancing the ferrimagnetic properties. Figure 2b shows an FESEM image of a film heated to 500 °C. Well-ordered nanoscale porosity is clearly observable. Figure 2c shows a mesoporous CFO framework heated to 700 °C. It is apparent from the image that the high-quality cubic mesoporous network still remains, even after this high-temperature crystallization.

More quantitative information on the structure of the mesoporous framework was obtained using 2D-SAXS. The data shown here were collected at angles of incidence, β (defined as the angle between the X-ray beam and the plane of the substrate), of 10° (off-grazing) and 90° (transmission). Figure 3 shows 2D-SAXS patterns for a KLE-templated CFO film before (250 °C) and after the onset of crystallization (500 and 700 °C). Samples with amorphous wall structure produce patterns with distinct scattering maxima. These maxima are characteristic of a distorted cubic pore structure, which is consistent with the electron microscopy data shown in Figure 2. We note that the lack of strong out-of-plane scattering maxima does not necessarily indicate a lack of out-of-plane order. Instead, the reduced scattering intensity in the out-of-plane direction likely arises from a combination of the fact that these thin films have only 10−15 repeat units in the direction normal to the substrate and the fact that a large β angle increases overall signal but biases the data against out-of-plane diffraction. The in-plane lattice parameter is approximately 25 nm, which is characteristic of KLE-templated sol−gel type metal oxide films.[43] The elliptical shape of the patterns further indicates lattice contraction of the cubic architecture normal to the substrate. A decrease in inorganic volume of more than 60% was determined for films heated above 250 °C. This contraction results in nonspherical pores and an isotropic stress (imposed by the substrate), which will become important in the following section on magnetic properties.

Upon heating films to 700 °C a loss of out-of-plane scattering was observed, though the in-plane scattering remained. The loss of the already weak out-of-plane scattering is likely due both to the lattice contraction and to the crystallization of the initially amorphous walls, which may

DOI: 10.1021/nl1014266 | *Nano Lett.* **XXXX,** *xxx,* 000–000

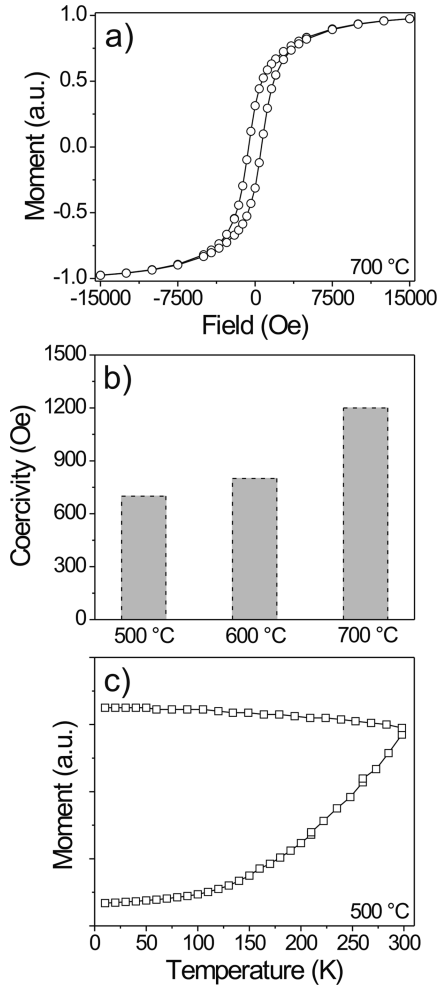

FIGURE 4. (a) Room temperature magnetic hysteresis experiments indicate that the CFO frameworks are ferrimagnetic. (b) The room temperature coercive widths increase as the domains grow from 700 Oe at 500 °C to 1200 Oe at 700 °C. (c) ZFC-FC measurements obtained on a film heated to 500 °C indicate that the magnetic domains of the mesoporous $CoFe_2O_4$ frameworks are strongly coupled.

slightly disrupt the nanoscale periodicity. The in-plane scattering is still strong, however, indicating the persistence of a network of ordered pores.[43] In agreement, experiments conducted in transmission mode on films heated to 700 °C (Figure 3, inset) reveal isotropic diffraction rings; thereby verifying good in-plane order. Overall, the 2D-SAXS data collectively verify that the pore structure is retained when the ferrimagnetic phase is achieved.

Using a SQUID magnetometer, the magnetic properties of the CFO frameworks were investigated. Figure 4a shows a typical magnetic hysteresis curve obtained at room temperature on a mesoporous CFO film heated to 700 °C. The width of these curves at the origin gives the coercivity, which is a measure of the magnetic energy needed to flip the spin direction in the system. For systems that have higher coercivity, the magnetization must be stable against both thermal fluctuations and demagnetizing interactions (i.e., antiferromagnetic coupling between domains). The typical way to raise the coercivity of a system is to increasing magnetic anisotropy. This anisoptroy includes shape, magnetocrystalline, or strain anisotropy. Figure 4b shows the variation of coercivity with thermal annealing temperature.

From the data in parts a and b of Figure 4, it can be seen that the mesoporous CFO framework is indeed a room temperature ferrimagnet. Even at the onset of crystallization (here 500 °C), the material has a coercivity of 700 Oe. As the crystalline domains grow larger at the higher annealing temperatures, the system shows a progressive increase in coercivity. This is because when the domains grow and the volumes increase, the overall magnetic energy, KV, increases and this raises the spin reversal energy of the system.[44] Here K is the anisotropy constant and V is the volume of a magnetic domain. We note, however, that isolated CFO nanodomains in the size ranges shown here usually exhibit superparamagnetic behavior. Moreover, 3D coupling of these magnetic domains generally results in demagnetizing interactions and thus causes a reduction in coercive width.[45] The fact that moderate ferrimagnetism is observed at room temperature implies strong coupling between domains to form larger magnetic regions that are resistant to thermal fluctuations without the reduction in coercivity that normally accompanies this coupling.[45] We speculate that this arises from the unique pore−solid architecture of these materials that leaves domains situated at the edge of a pore at least partly uncompensated. In all cases, however, the remanent magnetization is quite low, indicating that some demagnetizing interactions, i.e., antiferromagnetic coupling between magnetic domains, are indeed present in these materials. Despite this fact, the results show that all mesoporous crystalline samples employed in this work are room temperature ferrimagnets and that the magnetic coercivities of these mesoporous films can be readily tuned by thermal annealing.

To learn more about magnetic coupling between domains in these porous magnets, we can also explore temperature-dependent magnetization. Figure 4c shows a zero field cooled, field cooled (ZFC-FC) curve for a mesoporous CFO framework heated to 500 °C. By looking at the ZFC-FC curves, we can learn how thermal fluctuations affect the magnetization; this is typically an important factor when considering magnetic applications at room temperature. In the typical experiment, the sample is first cooled under zero field and then a small magnetic field is applied and magnetization is recorded as a function of increasing temperature. Initially, the domains are in a random state and so the sample starts off with a low moment. At low temperatures, even in the presence of the field, the spins are unable to align because the barrier for spin flip is greater than the thermal energy. Upon heating the sample, thermal energy frees the frozen spins and allows them to align with the field, thereby increasing the magnetization. Once all spins are free, thermal disordering takes over and the magnetization decreases. The transition from increasing to decreasing magnetization

DOI: 10.1021/nl1014266 | *Nano Lett.* **XXXX,** *xxx,* 000–000

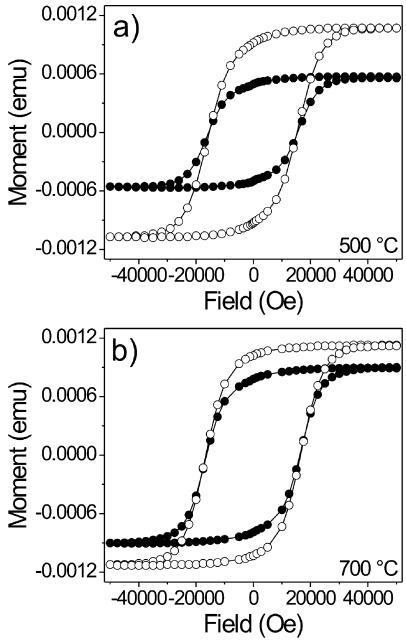

FIGURE 5. Orientation dependent hysteresis experiments conducted at 10 K show a larger saturation magnetization for films oriented perpendicular to the external magnetic field (open symbols) than for films with the plane of the substrate parallel to the applied field (solid symbols). This anisotropy is reduced when films are annealed at higher temperatures; similar results are obtained at room temperature.

is called the blocking temperature and isolated 12 nm CFO nanocrystals should show a blocking temperature below 100 K.[46]

From the data in Figure 4c, it is seen that the curve continually rises and even at room temperature there is no decrease in the overall magnetization. This further indicates that the magnetic domains are strongly coupled in a way that suppresses thermal fluctuations up to room temperature, thereby giving rise to ferrimagnetic behavior. In the FC curve, the sample is cooled while in the presence of the magnetic field in order to see how the removal of thermal energy affects the magnetization. In agreement with the ZFC data, the FC data show that the decrease in temperature has very little affect on the sample's magnetization because thermal fluctuations are already strongly suppressed.

To probe magnetic anisotropy in the CFO frameworks, the films were oriented both parallel and perpendicular relative to the external magnetic field of the magnetometer (Figure 5). It was observed that orientation has no effect on the coercive widths of the films, but the saturation magnetization values were different for the two orientations. The perpendicular direction yields a higher saturation magnetization compared to the parallel direction. This indicates that the easy axis for magnetic alignment in these films lies normal to the substrate. Thermal annealing at higher temperatures relaxes this anisotropy and brings the parallel and perpendicular saturation magnetization values closer together. The data presented in Figure 5 were collected at 10 K, and thus the coercive widths are quite large. The same trends in saturation magnetization are also observed for data collected at room temperature, however.

While the trends in the data are quite clear, this finding is contrary to the normal behavior in magnetic thin films, where the easy axes lie parallel to the substrate due to shape anisotropy. The dominant perpendicular magnetization indicates that there is another competing magnetic anisotropy within these mesoporous films that can overcome the shape anisotropy to produce an easy axis for magnetic alignment normal to the substrate. One possibility might be that shape anisotropy within the pore walls, rather than in the film as a whole, causes a preference for the out-of-plane magnetization. While this possibility cannot be ruled out, the data in Figure 3 indicate that the pores in these films are not spheres but are instead oblate spheroids with the long axes lying in the plane of the film. A framework of such pores would thus be more likely to show in-plane, rather than out-of-plane shape anisotropy.

Another possible explanation can be found in previous studies on strained epitaxial CFO films.[47] It has been observed that for dense CFO below a critical thickness, the application of sufficient in-plane tensile strains can distort the cubic lattices and reorient the magnetic easy axis to a dire normal to the plane of the film.[48,49] This result is in good agreement with the fact that CFO is known to show negative magnetostrictive behavior and so an in-plane tensile strain should cause the magnetization to align orthogonal to the tensile direction, resulting in magnetization perpendicular to the substrate.[49,50]

To investigate if the perpendicular magnetization in these mesoporous CFO films stems from similar distortions in the cubic crystal structure, synchrotron based high-angle XRD was used to probe the differences in the in-plane (derived from planes normal to the plane of the substrate) and out-of-plane (derived from planes parallel to substrate) atomic-scale lattice spacings. In this experiment, the lattice spacings are measured as the film substrate is rotated starting from the 90° (out-of-plane) orientation to the 180° (in-plane) orientation, at increments of 10° (Figure 6).

The angular-dependent XRD data was collected on the (311) lattice planes at two different annealing temperatures. For samples heated to both 600 and 650 °C, the overall trends are the same; the out-of-plane lattice spacing is the smallest and, as the film is rotated, there is a progressive increase in the lattice spacings. The in-plane spacing shows the largest value. Comparison of the equilibrium lattice spacing (2.5305 Å) with those at different angles for the mesoporous CFO at 600 °C shows that if we assume ideal stoichiometry in our films, there is a compression of the planes at 90° and a expansion of the planes at ~180°. In other words, the film is under tension in the plane of the substrate, similarly to the dense epitaxial CFO films that also show a preference for perpendicular magnetization. In a negative magnetostrictive material like CFO, this strain

DOI: 10.1021/nl1014266 | *Nano Lett.* **XXXX,** *xxx,* 000–000

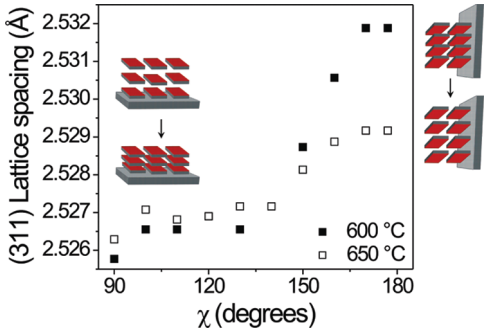

FIGURE 6. High-angle XRD experiments where the angle between the plane of the substrate and the incident beam, χ, was varied from 90 to 180°. The results show that the lattice constant in the plane of the film is larger than the lattice constant normal to the substrate, indicating an in-plane tensile strain. Annealing at higher temperature relaxes the expansive strain. As $CoFe_2O_4$ is magnetostrictive, these results can be used to explain both the propensity for out-of-plane magnetization and the reduction in this effect with increased thermal annealing.

forces the magnetic easy axes to lie orthogonal to the tension direction or parallel to the compression direction, which produces the perpendicular magnetization observed in Figure 5.

In the case of the mesoporous CFO samples heated to 650 °C, the trend is similar except that the additional heating relaxes some of the lattice strain and so the in-plane lattice spacings levels off at a value of 2.5295 Å which is quite close to the equilibrium lattice constant for single crystal CFO. While this film still shows strain anisotropy and thus should show a preference for magnetization normal to the substrate, the difference in the parallel and perpendicular lattice constants is much less than that for the film heated to 600 °C, and so less magnetic anisotropy is expected. Examination of the data in Figure 5 show that this trend is indeed observed. The excellent correlation between the thermally induced trends in Figures 5 and 6 argue that the origin of the out-of-plane magnetization is indeed lattice strain anisotropy, rather than some type of shape anisotropy in the pore walls.

We note that slightly off stoichiometry in our films or simply the Laplace pressure from being a nanoscale material could shift the equilibrium lattice spacing slightly.[51,52] Indeed, a logical value for the equilibrium lattice spacing would be the out-of-plane value observed in both films of 2.5267 Å. In this case, the films would be relaxed normal to the substrate and under tension in the plane of the film. Regardless of the true equilibrium value, however, we can draw the same conclusions about magnetic anisotropy. As long as the films show an in-plane lattice constant that is greater than the out-of-plane value, they should show a preference for magnetic alignment perpendicular to the substrate, regardless of where the equilibrium value lies.

For a variety of applications, a preference for out-of-plane magnetization is desirable. The complex epitaxial matching required to induce this perpendicular magnetic orientation in bulk CFO films, however, limits the systems where this can be achieved. For our nanoporous CFO, however, this orientation of the magnetic easy axis can be achieved on any substrate because the strain anisotropy comes not from lattice mismatch but instead from the nanoscale architecture itself. As formed, the amorphous inorganic framework of the CFO film has a relatively low density. Upon crystallization, this wall density increases, and because the film is bound to the substrate, this density increase results in a tensile strain. Part or all of this strain normal to the substrate is relaxed by flexing of the pores[53] and transformation from spherical to oblate (Figure 3). As the film is covalently bound to the substrate, this kind of pore flexing cannot take place in-plane and so tensile strain in the lattice results in anisotropy, which provides a facile way to produce a magnetic easy axis oriented perpendicular to the film in CFO on virtually any substrate.

Conclusion. Here we have demonstrated that mesoporous cobalt ferrite thin films can be templated using large diblock copolymers to produce nanoporous room temperature ferrimagnetic materials. These nanoporous magnets show reasonable coercivities that are tunable by thermal annealing conditions. In addition to the enhanced magnetic coercivities, the nanoscale architecture imparts a strain anisotropy to the material that overcomes the common in-plane shape anisotropy of thin films to produce a magnetic easy axis that is orthogonal to the plane of the substrate. This is a useful quality that often requires epitaxially grown thin films. It is envisioned that these interconnected pore networks with both high surface area and large pore volume will serve as exciting new materials for host–guest applications and magnetically exchange-coupled composites.

Acknowledgment. The authors would like to thank Dr. M. F. Toney and Dr. J. Pople at the Stanford Synchrotron Radiation Light Source for their technical support with XRD measurements. This work was supported by the Western Institute of Nanoelectronics which is sponsored by NERC (NRI), Intel, and the UC Discovery Program. T.B. acknowledges the support of a Liebig fellowship by the Fonds der Chemischen Industrie. Portions of this research were carried out at the Stanford Synchrotron Radiation Laboratory, a national user facility operated by Stanford University on behalf of the U.S. Department of Energy, Office of Basic Energy Sciences.

REFERENCES AND NOTES

(1) Comstock, R. L. *J. Mater. Sci.: Mater. Electron.* **2002**, *13*, 509.
(2) Piraux, L.; George, J. M.; Despres, J. F.; Leroy, C.; Ferain, E.; Legras, R.; Ounadjela, K.; Fert, A. *Appl. Phys. Lett.* **1994**, *65*, 2484.
(3) Lee, J. G.; Park, J. Y.; Oh, Y. J.; Kim, C. S. *J. Appl. Phys.* **1998**, *84*, 2801.
(4) Morber, J. R.; Ding, Y.; Haluska, M. S.; Li, Y.; Liu, P.; Wang, Z. L.; Snyder, R. L. *J. Phys. Chem. B* **2006**, *110*, 21672.
(5) Tirosh, E.; Markovich, G. *Adv. Mater.* **2007**, *19*, 2608.
(6) Cordente, N.; Respaud, M.; Senocq, F.; Casanove, M. J.; Amiens, C.; Chaudret, B. *Nano Lett.* **2001**, *1*, 565.
(7) Puntes, V. F.; Krishnan, K. M.; Alivisatos, A. P. *Science* **2001**, *291*, 2115.

DOI: 10.1021/nl1014266 | *Nano Lett.* **XXXX,** *xxx,* 000–000

(8) Sun, S. H.; Murray, C. B.; Weller, D.; Folks, L.; Moser, A. *Science* **2000**, *287*, 1989.
(9) Lin, X. M.; Samia, A. C. S. *J. Magn. Magn. Mater.* **2006**, *305*, 100.
(10) Fried, T.; Shemer, G.; Markovich, G. *Adv. Mater.* **2001**, *13*, 1158.
(11) Poddar, P.; Telem-Shafir, T.; Fried, T.; Markovich, G. *Phys. Rev. B* **2002**, *66*, No. 060403.
(12) Sun, S. H.; Murray, C. B. *J. Appl. Phys.* **1999**, *84*, 4325.
(13) Long, J. W.; Logan, M. S.; Rhodes, C. P.; Carpenter, E. E.; Stroud, R. M.; Rolinson, D. R. *J. Am. Chem. Soc.* **2004**, *126*, 16879.
(14) Long, J. W.; Logan, M. S.; Carpenter, E. E.; Rolinson, D. R. *J. Non-Cryst. Solids* **2004**, *350*, 182.
(15) Pettigrew, K. A.; Long, J. W.; Carpenter, E. E.; Baker, C. C.; Lytle, J. C.; Chervin, C. N.; Logan, M. S.; Stroud, R. M.; Rolinson, D. R. *ACS Nano* **2009**, *2*, 784.
(16) Kuliokowski, J.; Lenniwski, A. J. *J. Magn. Magn. Mater.* **1980**, *19*, 117.
(17) Pillai, V.; Shah, D. O. *J. Magn. Magn. Mater.* **1996**, *163*, 243.
(18) Srinivasan, G.; Rasmussen, E. T.; Hayes, R. *Phys. Rev. B* **2003**, *67*, No. 014418.
(19) Sim, C. H.; Pan, A. Z. Z.; Wang, J. *J. Appl. Phys.* **2008**, *103*, 124109.
(20) Liu, M.; Li, X.; Lou, J.; Zheng, S.; Du, K.; Sun, N. X. *J. Appl. Phys.* **2007**, *102*, No. 083911.
(21) Pasquale, M. *Sens. Actuators* **2003**, *104*, 142.
(22) Slonecweski, J. C. *J. Appl. Phys.* **1961**, *52*, 253.
(23) Li, S.; John, V. T.; O'Connor, C.; Harris, V.; Carpenter, E. *J. Appl. Phys.* **2000**, *87*, 6223.
(24) Meron, T.; Rosenberg, Y.; Lereah, Y.; Markovich, G. *J. Magn. Magn. Mater.* **2005**, *292*, 11.
(25) Tirosh, E.; Shemer, G.; Markovich, G. *Chem. Mater.* **2006**, *18*, 465.
(26) Ji, G.; Tang, S. L.; Ren, S. K.; Zhang, F. M.; Gu, B. X.; Du, Y. W. *J. Cryst. Growth* **2004**, *270*, 156.
(27) Ji, G.; Tang, S.; Xu, B.; Gu, B.; Du, Y. *Chem. Phys. Lett.* **2003**, *379*, 484.
(28) Richman, E. K.; Brezesinski, T.; Tolbert, S. H. *Nat. Mater.* **2008**, *7*, 712.
(29) Beck, J. S.; Vartuli, J. C.; Roth, W. J.; Leonowicz, M. E.; Kresge, C. T.; Schmitt, K. D.; Chu, C. T. W.; Olson, D. H.; Sheppard, E. W.; McCullen, S. B.; Higgins, J. B.; Schlenker, J. L. *J. Am. Chem. Soc.* **1992**, *114*, 10834.
(30) Zhang, J.; Deng, Y.; Wie, J.; Sun, Z.; Gu, D.; Bongard, H.; Liu, C.; Wu, H.; Tu, B.; Schuth, F.; Zhao, D. *Chem. Mater.* **2009**, *21*, 3996.
(31) Petkov, N.; Platschek, B.; Morris, M.; Holmes, J. D.; Bein, T. *Chem. Mater.* **2007**, *19*, 1376.
(32) Lee, J.; Orilall, M. J.; Warren, S. C.; Kamperman, M.; DiSalvo, F. J.; Wiesner, U. *Nat. Mater.* **2008**, *7*, 222.
(33) Ogawa, M. *J. Am. Chem. Soc.* **1994**, *116*, 7941.
(34) Brinker, J.; Lu, Y.; Sellinger, A.; Fan, H. *Adv. Mater.* **1999**, *11*, 579.
(35) Brezesinski, T.; Groenewolt, M.; Gibaud, A.; Pinna, N.; Antonietti, M.; Smarsly, B. M. *Adv. Mater.* **2006**, *18*, 2260.
(36) Mamak, M.; Coombs, N.; Ozin, G. *Adv. Mater.* **2000**, *12*, 198.
(37) Yang, P.; Deng, T.; Zhao, D.; Feng, P.; Pine, D.; Chmelka, B.; Whitesides, G.; Stucky, G. D. *Science* **1998**, *282*, 2244.
(38) Fattakhova-Rohlfing, D.; Brezesinski, T.; Rathousky, J.; Feldhoff, A.; Oekermann, T.; Wark, M.; Smarsly, B. *Adv. Mater.* **2006**, *18*, 2980.
(39) Sanchez, C.; Boissiere, C.; Grosso, D.; Laberty, C.; Nicole, L. *Chem. Mater.* **2008**, *20*, 682.
(40) Sallard, S.; Brezesinski, T.; Smarsly, B. M. *J. Phys. Chem. C* **2007**, *111*, 7200.
(41) Brezesinski, T.; Wang, J.; Tolbert, S. H.; Dunn, B. *Nat. Mater.* **2010**, *9*, 146.
(42) Richman, E. K.; Kang, C. B.; Brezesinski, T.; Tolbert, S. H. *Nano Lett.* **2008**, *8*, 3075.
(43) Brezesinski, T.; Wang, J.; Polleux, J.; Dunn, B.; Tolbert, S. H. *J. Am. Chem. Soc.* **2009**, *131*, 1802.
(44) Weller, D.; Moser, A. *IEEE Trans. Magn.* **1999**, 354423.
(45) Gross, A. F.; Diehl, M. R.; Beverly, K. C.; Richman, E.; Tolbert, S. H. *J. Phys. Chem. B* **2003**, *10*, 5475.
(46) Li, S. C.; Liu, L. M.; John, V. T.; O'Connor, C. J.; Harris, V. G. *IEEE Trans. Magn.* **2001**, *37*, 2350.
(47) Suzuki, Y.; Hu, G.; van Dover, R. B.; Cava, R. J. *J. Magn. Magn. Mater.* **1999**, *191*, 1.
(48) Lisfi, A.; Williams, C. M. *J. Appl. Phys.* **2003**, *93*, 8143.
(49) Lisfi, A.; Williams, C. M.; Nguyen, L. T.; Lodder, J. C.; Coleman, A.; Corcoran, H.; Johnson, A.; Chang, P.; Kumar, A.; Morgan, W. *Phys. Rev. B* **2007**, *27*, No. 054405.
(50) Cheng, F.; Peng, Z.; Liao, C.; Xu, Z.; Gao, S.; Yan, C.; Wang, D.; Wang, J. *Solid State Commun.* **1998**, *107*, 471.
(51) Tolbert, S. H.; Alivisatos, A. P. *Annu. Rev. Phys. Chem.* **1995**, *46*, 595.
(52) Zhang, H.; Chen, B.; Banfield, J. F. *Phys. Chem. Chem. Phys.* **2009**, *11*, 2553.
(53) Kirsch, B. L.; Chen, X.; Richman, E. K.; Gupta, V.; Tolbert, S. H. *Adv. Funct. Mater.* **2005**, *15*, 1319.

DOI: 10.1021/nl1014266 | *Nano Lett.* **XXXX,** *xxx,* 000–000